

Electrodeposition of Palladium and Adsorption  
of Palladium Chloride onto Solid Electrodes from

94-29709

Room Temperature Molten Salts

Hugh C. De Long,\* J. S. Wilkes,\* and R. T. Carlin\*

Research Laboratory, United States Air Force Academy, Colorado 80840-6272

DTIC QUALITY INSPECTED 5

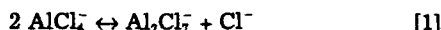
①

ABSTRACT

FJSRL-JR-94-0013

The electrodeposition of palladium onto various electrode surfaces was examined in room temperature  $\text{AlCl}_3$ -MEIC molten salts with  $\text{AlCl}_3$  mole fractions,  $N$ , from  $0.33 < N < 0.5$  (basic melts) to  $0.5 < N < 0.67$  (acidic melts) and at  $N = 0.5$  (neutral melt). The behavior of palladium electrodeposition was markedly dependent on the mole fraction of  $\text{AlCl}_3$  in the molten salts. The palladium reduction potential shifts approximately +2.0 V when the melt is changed from basic to acidic. Nucleation overpotentials were evident in basic melts, and to a lesser extent in acidic and neutral melts. In acidic melts, the reduction of the sparingly soluble palladium complex displays characteristics distinctive of an adsorption phenomenon, while the oxidation process shows considerable broadening. Oxidation of a palladium electrode in an  $N = 0.55$  acidic melt produces an insoluble palladium chloride layer (approximately a monolayer) on the electrode surface which protects the underlying metal from further oxidation. Reduction of this surface anchored palladium chloride layer is rapid and provides a high cathodic current density. This behavior in acidic melts is pointedly different from the reduction process in a basic melt where the reduction of the soluble palladium chloro complex exhibits a diffusion wave with nucleation effects.

Room temperature molten salts derived from  $\text{AlCl}_3$ -MEIC (MEIC = 1-methyl-3-ethylimidazolium chloride) are of interest for battery applications due to their wide liquidus range and high conductivity.<sup>1,2</sup> In addition, the adjustable Lewis acidity of these melts introduces a unique means to alter solvent and solute electrochemistry dramatically by changing the mole ratio,  $N$ , of  $\text{AlCl}_3$  to MEIC. The predominant equilibrium controlling the anion speciation in these melts is given by



where  $K_{\text{eq}} = 10^{-17}$ ; therefore, basic melts ( $0.33 < N < 0.5$ ) contain excess  $\text{Cl}^-$  and acidic melts ( $0.5 < N < 0.67$ ) contain the Lewis acidic species  $\text{Al}_2\text{Cl}_7^-$ .<sup>1</sup> Equation 1 is qualitatively and quantitatively analogous to water autoionization ( $K_{\text{eq}} = 10^{-14}$ ), where, like the hydronium ion,  $\text{Al}_2\text{Cl}_7^-$  is the acidic species and, like the hydroxide ion,  $\text{Cl}^-$  is the basic species. The speciation in acidic melt is often dramatically different than in basic melt, just as they are in aqueous solvents.

Understanding the behavior of materials in room temperature molten salts is an important step in assessing their suitability for use as electrodes in follow-on battery development. Some materials have been looked at, to varying degrees, in  $\text{AlCl}_3$ -MEIC molten salt systems.<sup>3,4</sup> The examination of metal chlorides for battery applications indicates that they exhibit different behavior depending on whether the melt composition is basic or acidic. Certain metal chlorides that are soluble in basic melts are only slightly soluble, or insoluble, in acidic melts. The less-soluble nature of metal chlorides in acidic melts may lead to adsorption effects on the electrode surface.<sup>5</sup>

The electrochemistry of palladium chloride was first examined in basic  $\text{AlCl}_3$ -MEIC melts by Hussey *et al.*<sup>6</sup> They discovered that palladium exists as  $\text{PdCl}_4^{2-}$  and undergoes a two-electron reduction in basic melts. The reduction is limited kinetically by a three-dimensional nucleation process. This is accompanied by an unusual two-peak oxidation which has not been fully explained.

While palladium chloride is soluble in basic melt, it is only slightly soluble in acidic and neutral melts.<sup>7,8</sup> This low solubility leads to adsorption of a Pd(II) chloride complex onto solid electrode surfaces and substantially alters the Pd(II)/Pd electrochemical couple. In addition, the electrochemistry of a Pd electrode in acidic and neutral melts consists exclusively of surface redox processes similar to the behavior of Pd in aqueous electrolytes.<sup>9-11</sup> Here, we ex-

amine the surface electrochemistry of the Pd electrode as well as the adsorption of Pd(II) chloro complex on several different solid electrodes.

## Experimental

Purification of melt components has been described previously.<sup>12,13</sup>  $\text{PdCl}_2$  (Aldrich, 99.999%) was used without further purification. All experiments were performed at room temperature in a Vacuum Atmospheres glove box under a UHP helium atmosphere.

Melts were prepared by slowly combining calculated quantities of MEIC and  $\text{AlCl}_3$ . Protonic impurities were removed from the melts by addition of  $\text{EtAlCl}_2$  or by vacuum treatment at  $1 \times 10^{-5}$  Torr for several days.<sup>14,15</sup> All  $\text{AlCl}_3$ -MEIC melts containing palladium ions were prepared by addition of  $\text{PdCl}_2$  or  $(\text{MEI})_2\text{PdCl}_4$  to the melt.  $(\text{MEI})_2\text{PdCl}_4$  is a new salt produced by adding  $\text{PdCl}_2$  to MEIC and heating to  $150^\circ\text{C}$ .<sup>16</sup> Use of  $(\text{MEI})_2\text{PdCl}_4$  facilitates dissolution of Pd(II) into the  $\text{AlCl}_3$ -MEIC melts. Addition of brick red  $\text{PdCl}_2$  to basic  $\text{AlCl}_3$ -MEIC melts gave a yellow-orange coloration, while addition of  $\text{PdCl}_2$  to acidic and neutral melts produced a red coloration. Due to the low solubility of  $\text{PdCl}_2$  in the acidic and neutral melts, these melts became saturated before all the  $\text{PdCl}_2$  was dissolved. Heating the melts at  $95^\circ\text{C}$  for 1 week helped dissolve more of the  $\text{PdCl}_2$ . The solubility of  $\text{PdCl}_2$  was greater in the most acidic melt ( $N = 0.67$ ), but decreased as the melts tended toward neutral. The solubility of  $\text{PdCl}_2$  decreased in the order basic  $\gg$  acidic ( $N = 0.67$ )  $>$  acidic ( $N = 0.55$ )  $\geq$  neutral ( $N = 0.50$ ).

Several different working electrodes were used in this investigation. Several polycrystalline palladium, platinum, and tungsten metal disk electrodes were constructed by sealing the appropriate wire (Aldrich) in glass tubes, cutting the glass to expose a circular disk electrode, and then polishing the electrode surface with a Struers DAP-V grinder-polisher using diamond pastes. The geometric areas of the resulting palladium, platinum, and tungsten disk electrodes were  $7.85 \times 10^{-3}$ ,  $7.85 \times 10^{-3}$ , and  $0.96 \times 10^{-3}$   $\text{cm}^2$ , respectively. Rotating disk glassy carbon, palladium, and platinum electrodes were purchased from Pine Instrument Co. and were all reported by the manufacturer to have a geometric surface area of  $0.1984 \text{ cm}^2$ . Rotating disk tungsten electrodes from Pine Instrument Co. had geometric areas of  $0.2815 \text{ cm}^2$  and  $0.2822 \text{ cm}^2$ . Glassy carbon (3 mm diam) and gold (1.65 mm diam) electrodes were purchased from BAS and Sargent Welch, respectively.

For all electrochemical experiments, the counterelectrode was a platinum foil, and the reference electrode con-

DISTRIBUTION STATEMENT A

Approved for public release

Distribution Unlimited

94 9 12 084

sisted of Al wire immersed in either an  $N = 0.67$  or  $N = 0.60$   $\text{AlCl}_3$ -MEIC melt contained in separate fritted or Vycor glass compartments. Cyclic staircase voltammetry was performed with a (Princeton Applied Research) PARC Model 273 potentiostat/galvanostat controlled with the M270/4 software package. Ramp mode was used for data acquisition to simulate linear scan voltammetry as closely as possible. Rotating disk experiments were performed with a Pine Instrument Co. Model AFMSRX rotator, and PARC Model 273 potentiostat/galvanostat controlled with the M270/4 software package. UV-vis spectra were obtained inside the glove box using a Guided Wave fiber optic system.

### Results and Discussion

**Basic melts.**—Palladium deposition-stripping behavior was the same on all the metal electrodes tested; platinum, tungsten, glassy carbon, and gold, except palladium. Cyclic staircase voltammetry of palladium deposition-stripping behavior in an  $N = 0.444$  melt is shown in Fig. 1 at a Pine Instruments rotating disk (RDE) glassy carbon electrode, which is typical for palladium in all basic melts. An obvious feature is the negative overpotential seen for the Pd(II) reduction wave; a result of a nucleation phenomenon typical for many metal electrodeposition processes.<sup>17</sup> At a palladium electrode, Fig. 2, the waves for the reduction of Pd(II) from solution are broader than on other electrodes, and the oxidation at 0.15 V probably corresponds to oxidation of Pd metal to  $\text{PdCl}_2^-$ , i.e., the Pd electrode does not passivate in basic melts as it does in neutral and acidic melts (*vide infra*). When the scan is reversed after Pd anodization, a reduction peak at  $-0.75$  V, corresponding to reduction of Pd(II) to Pd, appears and increases when the switching potential is more positive.

RDE experiments were performed at a glassy carbon electrode in an  $N = 0.33$  basic melt containing dissolved  $\text{PdCl}_2$  ( $[\text{Pd(II)}] = 1.7 \times 10^{-2} \text{ M}$ ). Rotation rates were varied from 100 to 2400 rpm. The basic melt showed a diffusion-limited current from 200 to 2400 rpm. From 200 to 400 rpm, a small peak at the beginning of the limiting plateau was observed indicative of adsorption of the Pd(II) complex on the electrode prior to reduction; this peak was not apparent in the faster rotation voltammograms.

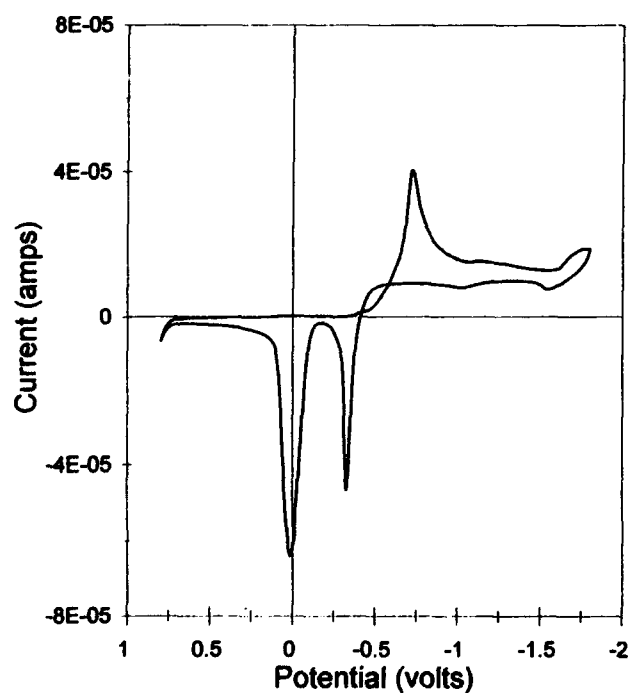


Fig. 1. Cyclic staircase voltammogram of Pd(II)/Pd couple on glassy carbon in basic melt ( $N = 0.444$ ) with a scan rate of 1 mV/s. Referenced to an aluminum wire in  $N = 0.67$   $\text{AlCl}_3$ -MEIC.

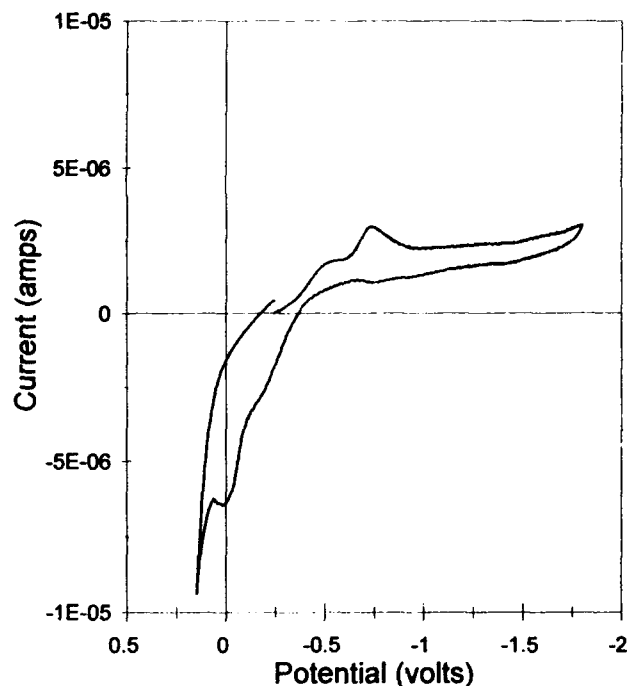


Fig. 2. Cyclic staircase voltammogram of Pd(II)/Pd couple on palladium in basic melt ( $N = 0.444$ ) with a scan rate of 1 mV/s. Referenced to an aluminum wire in  $N = 0.67$   $\text{AlCl}_3$ -MEIC.

The two Pd oxidation waves seen in Fig. 1 were first described by Sun and Hussey.<sup>6</sup> They attributed the more negative wave to bulk Pd oxidation and the more positive wave to stripping of a chemisorbed layer.<sup>6</sup> This is in contradiction with their formal potential reported for the Pd(II)/Pd couple which falls between the two oxidation waves. Sun and Hussey reported a formal electrode potential of  $-0.230$  V in a 44.4% ( $N = 0.444$ ) melt while the two oxidation waves are seen at approximately  $-0.32$  and  $+0.05$  V in Fig. 2 of Ref. 6. If the more negative wave is bulk Pd oxidation, it is expected to have a larger area than the chemisorbed layer; however, the opposite is true. An alternate explanation becomes apparent when we realize that the more positive wave is at the same potential as bulk Pd oxidation observed for the Pd electrode in Fig. 2; therefore, the more positive wave corresponds to bulk Pd oxidation to Pd(II). The more negative wave may be oxidation of Pd to adsorbed  $\text{PdCl}_2^-$ ; the less positive potential for oxidation results from thermodynamic stabilization of the product by the adsorption phenomenon.<sup>5</sup> Consistent with this interpretation is that in the RDE studies of Pd(II) reduction described above,  $\text{PdCl}_2^-$  is adsorbed to the electrode surface giving an initial peak in the slow rotation RDE voltammetric responses.

**Acidic neutral melts.**—Cyclic staircase voltammograms for the Pd(II)/Pd couple in acidic and neutral  $\text{AlCl}_3$ -MEIC melts containing dissolved Pd(II) are shown in Fig. 3 to 5 at a palladium electrode. For the  $N = 0.67$  melt, the higher solubility of Pd(II) in this more acidic melt allowed for a stable open-circuit potential to be used as the starting potential. In the neutral and  $N = 0.55$  melts, the low solubility of Pd(II) gave an unstable open-circuit potential; therefore, scans were begun at a potential negative of the reduction wave. The shape of the curves were independent of the time held at the negative potential. For the  $N = 0.67$  melt, the Pd(II)/Pd reduction and oxidation waves are broad and only one oxidation process is observed. In the neutral melt, the palladium reduction wave is shifted more negative while the oxidation remains relatively unchanged, Fig. 4. At a melt composition of  $N = 0.55$ , the reduction wave in Fig. 5 has a full width at half-height (FWHH), of only 46.6 mV, while the oxidation remains broad. The three figures indicate the movement of the reduction wave to more

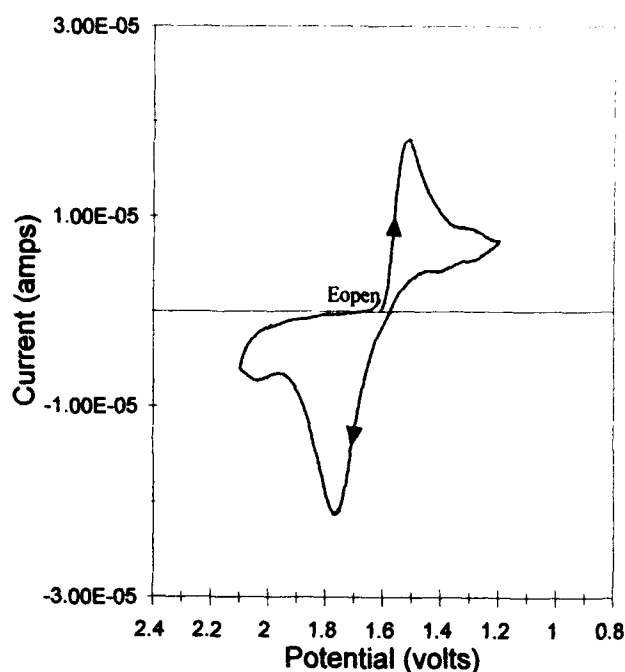


Fig. 3. Cyclic staircase voltammogram of Pd(II)/Pd couple on palladium in acidic melt ( $N = 0.67$ ) with a scan rate of 100 mV/s. Referenced to an aluminum wire in  $N = 0.60$  AlCl<sub>3</sub>-MEIC.

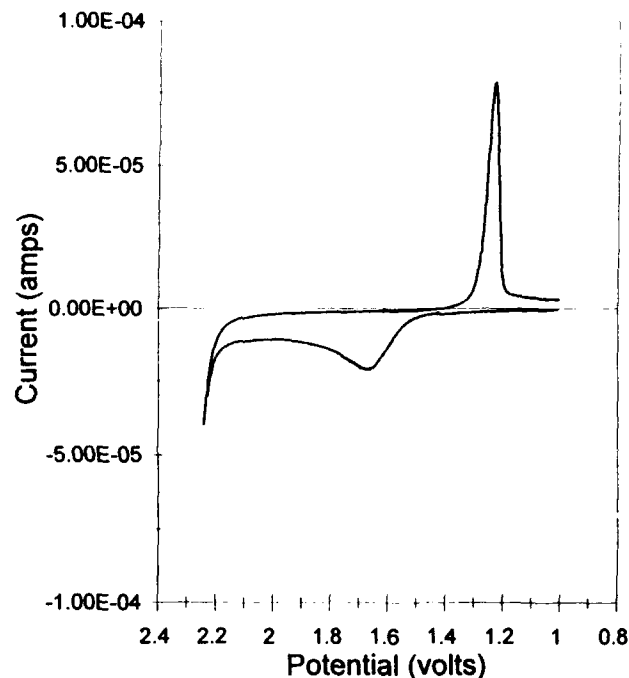


Fig. 5. Cyclic staircase voltammogram of Pd(II)/Pd couple on palladium in acidic melt ( $N = 0.55$ ) with a scan rate of 100 mV/s. Referenced to an aluminum wire in  $N = 0.60$  AlCl<sub>3</sub>-MEIC.

negative potentials as the melt composition is changed from  $N = 0.67$  to  $N = 0.50$ . Importantly, for the acidic and neutral melts, the palladium electrode does not undergo continuous oxidation as in the basic melts. Instead, a surface coating of an insoluble palladium chloride complex, designated PdCl<sub>2</sub>, passivates the surface toward further oxidation. The broadness of the oxidation is consistent with formation of an insoluble surface-bound complex. Similar behavior is observed for palladium electrodes in aqueous systems where palladium oxides/hydroxides are formed.<sup>9-11</sup> As discussed below, the behavior of palladium in the  $N = 0.55$  melt can be reproduced even when no Pd(II) has been added to the melt, *i.e.*, the phenomenon is a surface effect

and operates for bulk and electrodeposited palladium metal.

Palladium deposition-stripping behavior in acidic melts containing dissolved PdCl<sub>2</sub> appeared the same regardless of whether the electrode was platinum, tungsten, palladium, gold, or glassy carbon. The Pd(II)/Pd couple in an  $N = 0.55$  melt at glassy carbon is shown in Fig. 6. The oxidation process at +1.5 V is observed only after palladium metal has been electrodeposited onto the surface by an initial scan negative of the reduction wave at +1.1 V. As with the palladium electrode, the electrodeposited palladium is passivated, so only palladium at the surface of the electrodeposit

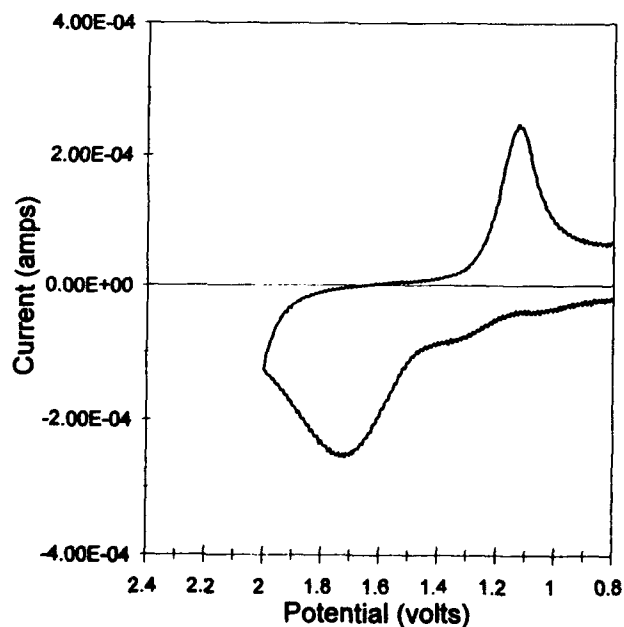


Fig. 4. Cyclic staircase voltammogram of Pd(II)/Pd couple on palladium in neutral melt ( $N = 0.50$ ) with a scan rate of 100 mV/s. Referenced to an aluminum wire in  $N = 0.60$  AlCl<sub>3</sub>-MEIC.

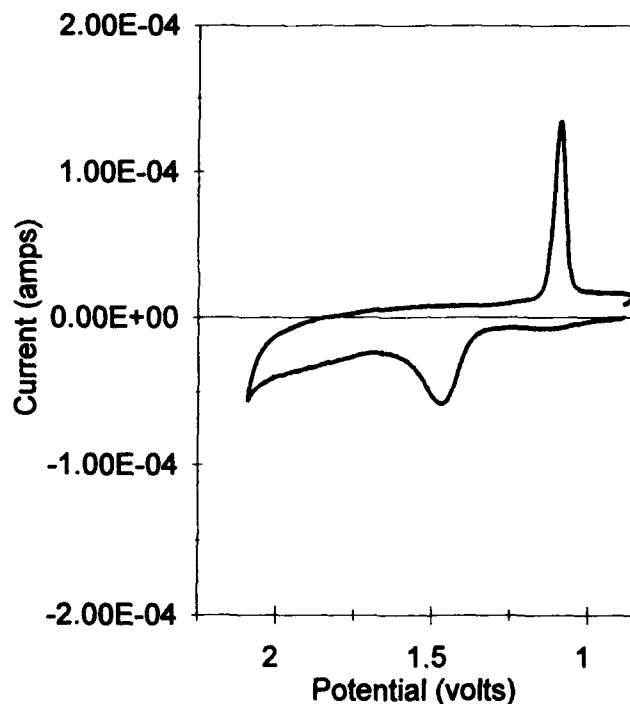


Fig. 6. Cyclic staircase voltammogram of Pd(II)/Pd couple on glassy carbon in acidic melt ( $N = 0.55$ ) with a scan rate of 100 mV/s. Referenced to an aluminum wire in  $N = 0.60$  AlCl<sub>3</sub>-MEIC.

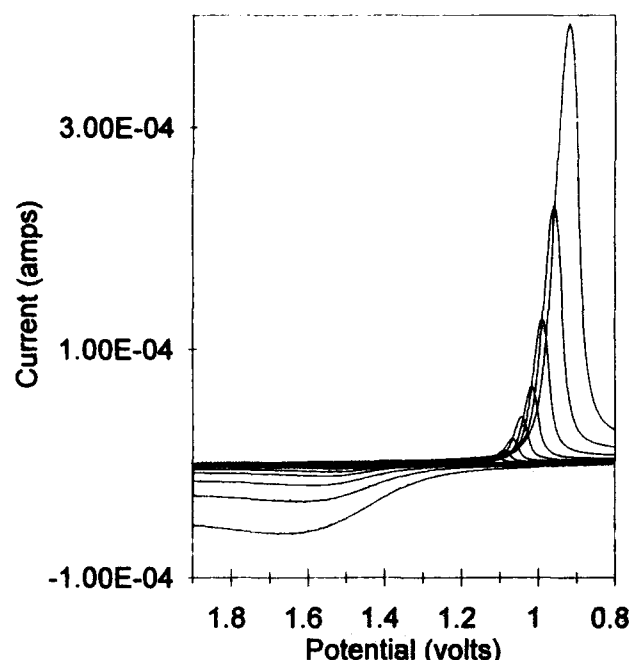


Fig. 7. Cyclic staircase scan rate study at a 0.1964 cm<sup>2</sup> Pd electrode in acidic melt (*N* = 0.55). Referenced to an aluminum wire in *N* = 0.60 AlCl<sub>3</sub>-MEIC. Scan rates are given in Table I.

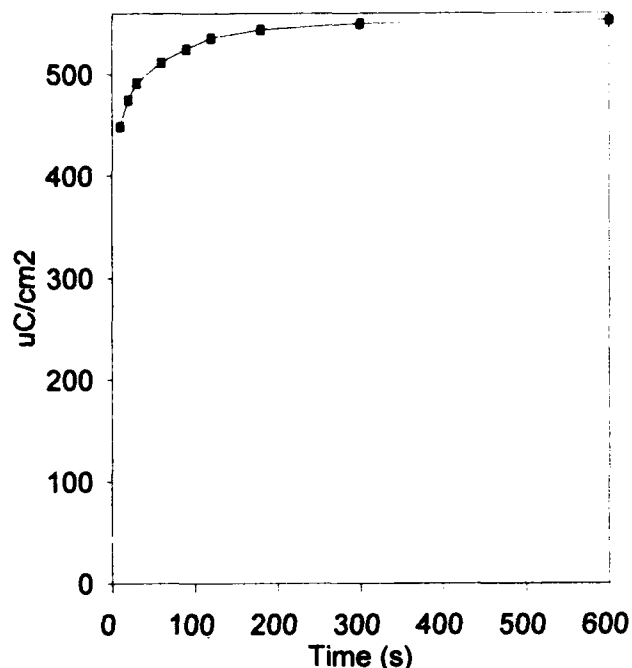


Fig. 8. Palladium surface coverage plot of integrated charge vs. time held at +1.9 V at a 0.1964 cm<sup>2</sup> Pd electrode. Referenced to an aluminum wire in *N* = 0.60 AlCl<sub>3</sub>-MEIC.

is electroactive. Therefore, optimal use of the palladium can be achieved when a thin palladium film on an inert substrate is employed.

Scan rate studies were performed on palladium reduction at a 0.1964 cm<sup>2</sup> Pd electrode in an *N* = 0.55 melt without dissolved PdCl<sub>2</sub>. Voltammetric scans were performed by initially scanning from +0.8 to +1.9 V, holding the potential at +1.9 V for 60 s, and then scanning negative through the reduction wave back to +0.8 V. Voltammograms at various scan rates are depicted in Fig. 7. Table I contains information on the scan rate (*v*), cathodic peak potential (*E*<sub>p</sub><sup>c</sup>), cathodic peak height (*i*<sub>p</sub><sup>c</sup>), and FWHH for the voltammograms in Fig. 7. The slope of log *v* vs. log *i*<sub>p</sub><sup>c</sup> is 0.96 for scan rates of 6.25 to 50 mV/s, indicating an adsorption process. For scan rates from 100 to 800 mV/s, a slight curvature is evident causing a deviation from linearity. This is due to kinetic limitations brought about by the nucleation phenomena discussed below. The kinetic limitations also cause the FWHH to increase and the *E*<sub>p</sub><sup>c</sup> to shift negatively with increasing scan rate.

RDE experiments were performed at a palladium electrode in an *N* = 0.55 melt containing no dissolved Pd(II). Rotation rates were varied from 100 to 2400 rpm. After full oxidation of the surface at +1.9 V, a negative scan revealed that the reduction wave was unchanged, independent of rotation rate, confirming the surface nature of the process.

Using a 0.1964 cm<sup>2</sup> Pd electrode in an *N* = 0.55 melt containing no dissolved PdCl<sub>2</sub>, it was possible to quantitate the adsorption process by studying the oxidation and reduction of the palladium electrode surface. This was done by holding the potential of the Pd electrode at +1.9 V for in-

creasing times, and then scanning the potential at 100 mV/s through the surface reduction at +1.2 V. Integration of the charge under the reduction peak provides a quantitation of the amount of PdCl<sub>2</sub> formed during the oxidation process. The cathodic charge plotted as a function of hold time is depicted in Fig. 8. Assuming a closest packed arrangement of palladium atoms at the electrode surface, the charge per unit area necessary to oxidize a monolayer of Pd(0) to Pd(II) is 4.94 × 10<sup>-4</sup> C/cm<sup>2</sup>. (A radius of 1.37 Å for Pd was used in the calculation.<sup>19</sup>) Therefore, the charge found for the Pd RDE electrode corresponds to formation of a single monolayer of PdCl<sub>2</sub> using a surface roughness of 1.1. Depending on the source of the Pd electrode, the calculated surface coverage was between 0.5 and 2 monolayers using a surface roughness of 1.1. This may be a result of a variable surface roughness for different electrode suppliers (*i.e.*, the surface roughness is not constant at 1.1 for different electrodes) or differences in the type and purity of Pd used by different manufacturers. However, for the same electrode source, the surface coverage was generally reproducible.

The reduction process at a 0.1964 cm<sup>2</sup> Pd electrode in an *N* = 0.55 melt containing no Pd(II) was studied as a function of the oxidizing potential. A series of experiments were performed in which the potential was scanned into the oxidation wave, held at different oxidizing potential for 60 or 180 s, and then scanned through the reduction wave. Voltammograms (*v* = 100 mV/s) collected for 60 s holds at the different oxidizing potentials are shown in Fig. 9. The results at a 0.1964 cm<sup>2</sup> Pd RDE electrode are summarized in Tables II and III. As the oxidizing potential becomes more positive, several observations are made: (i) the peak height and the charge under the reduction wave increase; (ii) the peak of the reduction wave shifts to negative potentials; and (iii) the reduction wave becomes narrower. The first observation indicates that oxidation at more positive potentials increases the amount of PdCl<sub>2</sub> formed on the Pd electrode surface. The second and third observations are inconsistent with a process controlled by electron transfer kinetics. For a two-electron process at 25°C, the FWHH for a reversible process is expected to be 45.3 mV, while the FWHH for an irreversible process with α = 0.5 should be 62.5 V.<sup>2</sup> At the most positive oxidation potential, the FWHH is less than that for a reversible system. The narrowing of the reduction wave with the negative reduction potential shift is opposite to that expected for electron-transfer ki-

Table I. Scan rate study of Pd(II) surface reduction in *N* = 0.55 AlCl<sub>3</sub>-MEIC at a 0.1964 cm<sup>2</sup> Pd electrode.

<i>v</i> (mV/s)	<i>E</i> <sub>p</sub> <sup>c</sup> (V)	<i>i</i> <sub>p</sub> <sup>c</sup> (μA)	FWHH (mV)
6.25	1.113	5.296	45.75
12.5	1.089	10.59	42.64
25	1.070	20.43	42.57
50	1.046	38.88	42.51
100	1.018	64.05	44.86
200	0.9910	122.49	48.85
400	0.9595	218.68	56.22
800	0.9210	372.78	69.10

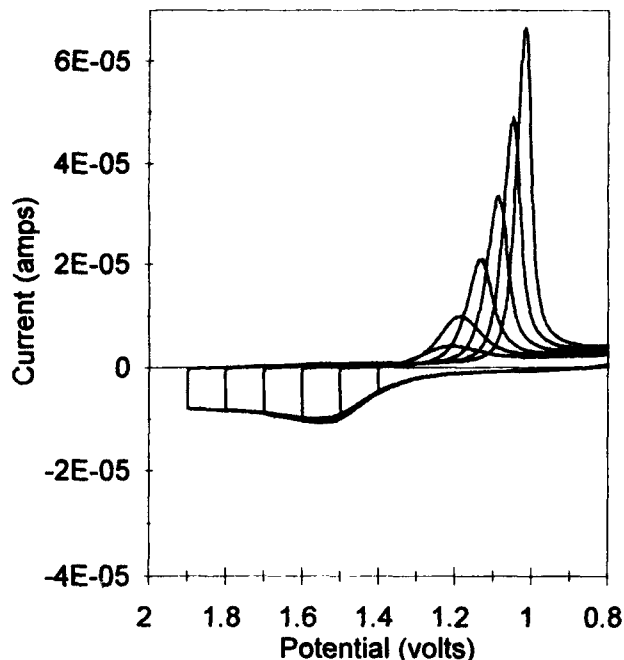


Fig. 9. Voltammogram series obtained for 60 s holds at oxidizing potentials of 1.9, 1.8, 1.7, 1.6, 1.5, and 1.4 V. Experiment accomplished with a 0.1964 cm<sup>2</sup> Pd electrode in acidic melt ( $N=0.55$ ) using a scan rate of 100 mV/s. Referenced to an aluminum wire in  $N=0.60$  AlCl<sub>3</sub>-MEC.

netics. Staircase voltammetry was used to obtain the data in Tables II and III, whereas, the theoretical FWHH values are derived for linear scan voltammetry. However, the use of ramp mode (step height < 0.5 mV) in the data acquisition setup simulates linear sweep voltammetry very well. In addition, varying the step height up to 5 mV and altering the current sampling parameters has minimal effect on  $i_p^*$  and FWHH. For a reversible surface process, this is not expected to be the case; instead, peak height has been shown to be a strong function of step height and current sampling parameters.<sup>19</sup> A continuous oscilloscope trace of a ramp mode staircase voltammogram is shown in Fig. 10 confirming the linear scan behavior of ramp mode. The curve mim-

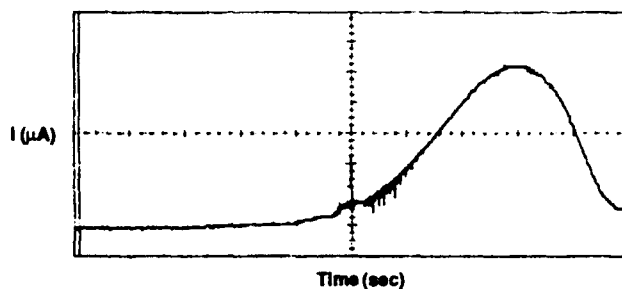


Fig. 10. Oscilloscopic trace of staircase voltammogram showing the result of using the ramp mode of the PAR M270 software and 273 potentiostat during palladium surface reduction: 20 s oxidation at +1.9 V.

ics a linear scan voltammogram; no potential steps, charging current spikes, or current decays are apparent.

Continuous oscilloscope traces of the staircase voltammograms were recorded for the reduction process following 20 s holds at oxidizing potentials of +1.9 and +1.65 V. The potential waveform parameters consisted of a 10 mV step height and a 100 ms step time giving a scan rate of 100 mV/s. The resulting traces shown in Fig. 11A and B reveal the behavior of the reduction process more clearly. The initial potential steps for the reduction in Fig. 11A (following oxidation at +1.9 V) show a gradual rise in the current as a function of time. This behavior is characteristic of a nucleation phenomenon.<sup>17</sup> More recent results indicate the reduction process is limited by a 2D nucleation phenomenon.<sup>8</sup> Such 2D nucleation involving interconversion of two solid phases at an electrode surface are analogous to nucleation processes observed during anodic film formation at a metal electrode.<sup>20</sup> Near the maximum in Fig. 11A, the current rise for each step becomes less pronounced, and the current transients begin to show more typical staircase behavior, i.e., an initial charging current followed by a current decay. However, the current transients behavior for all potential steps in Fig. 11B are typical for staircase voltammetric experiments. Therefore, as the oxidizing potential becomes less positive, kinetic limitations resulting from the nucleation phenomenon for the reduction process become less pronounced. Assuming the PdCl<sub>2</sub> to Pd reduction occurs via a lateral growth mechanism, it is necessary to have

Table II. Staircase voltammetry results for Pd(II) surface reduction as a function of 60 s holds at different oxidizing potentials using a 0.1964 cm<sup>2</sup> Pd electrode.

Oxidizing potential (V)	$E_p^c$ (V)	Charge (μC)	$i_p$ (mA)	FWHH (mV)
1.4	1.202	6.509	3.442	165.9
1.5	1.185	13.63	8.937	126.4
1.6	1.135	19.66	19.69	78.73
1.7	1.088	25.67	31.86	61.39
1.8	1.049	31.22	46.90	52.32
1.9	1.018	36.60	64.07	44.85

Table III. Staircase voltammetry results for Pd(II) surface reduction as a function of 180 s holds at different oxidizing potentials using a 0.1964 cm<sup>2</sup> Pd electrode.

Oxidizing potential (V)	$E_p^c$ (V)	Charge (μC)	$i_p$ (mA)	FWHH (mV)
1.4	1.196	9.373	4.944	163.5
1.5	1.156	21.86	18.25	99.85
1.6	1.107	30.75	33.41	74.51
1.7	1.063	37.61	50.12	61.35
1.8	1.028	43.86	70.45	51.08
1.9	1.004	50.38	89.00	45.59
2.0	0.9855	56.15	105.00	43.19
2.1	0.9804	64.18	118.3	43.08

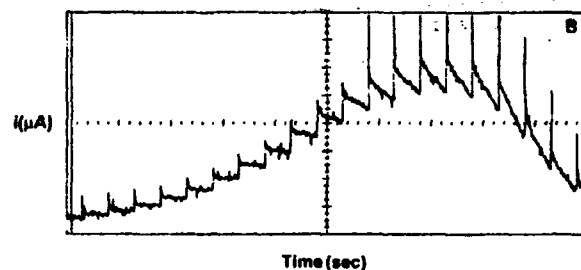
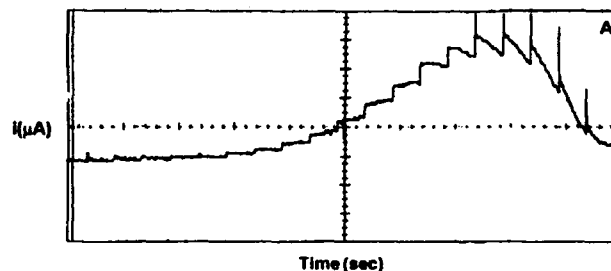


Fig. 11. Oscilloscopic traces of staircase voltammograms showing the individual steps during palladium surface reduction: (A) 20 s oxidation at +1.9 V, and (B) 20 s oxidation at +1.65 V.

Table IV. UV-vis absorption maxima (nm) for Pd(II) species.

PdCl <sub>2</sub> <sup>-</sup> HCl (aq) <sup>a</sup>	PdCl <sub>2</sub> <sup>-</sup> Basic melt <sup>b</sup>	Pd(AlCl <sub>4</sub> ) <sub>2</sub> Vapor phase <sup>c</sup>	Pd(II) Acidic melt
223	— <sup>d</sup>	—	— <sup>d</sup>
280	291	249	278
336 <sup>sh</sup>	345-347 <sup>sh</sup>	—	350-355 <sup>sh</sup>
474	480-483	500	500-504
619 <sup>w</sup>	620 <sup>w</sup>	—	—

sh = shoulder, w = weak.

<sup>a</sup>Ref. 21 and 22.<sup>b</sup>N = 0.33 (this work) and Ref. 6.<sup>c</sup>Ref. 23.<sup>d</sup>MEIC absorbance interference.

Pd metal growth centers already present, or to produce them via a nucleation process. For the most positive oxidizing potentials, the surface is fully converted to PdCl<sub>2</sub>; therefore, production of Pd metal sites requires an initial nucleation process. For less positive oxidizing potentials, Pd metal is still accessible at the surface to serve as sites for lateral growth, reducing the need for nucleation. The coulometric charges listed in Tables II and III are consistent with this interpretation. The changes in the FWHH as a function of oxidizing potential can be understood by recognizing that for more positive oxidizing potentials, it is more difficult to start the reduction, but after it has started, the reduction proceeds rapidly due to a higher thermodynamic overpotential. Therefore, the reduction peak shifts to negative potential and becomes narrower with more positive oxidizing potential as seen in Table III.

**UV-vis spectroscopy.**—A UV-vis spectrum was obtained for Pd(II) in the Lewis acidic molten salt, and the results are summarized in Table IV along with spectra for PdCl<sub>2</sub><sup>-</sup> in aqueous HCl<sup>21,22</sup> and basic melts<sup>6</sup> and for vapor phase Pd(AlCl<sub>4</sub>)<sub>2</sub>.<sup>23</sup> The spectrum of Pd(II) in the acidic melt more closely matches the spectrum of vapor phase Pd(AlCl<sub>4</sub>)<sub>2</sub> which has been assigned a square planar geometry.<sup>23</sup> In particular, both vapor phase and acidic melt Pd(II) species exhibit a metal centered  $d \leftarrow d$  transition at 500 nm; however, the  $L \leftarrow M$  charge-transfer band at 278 nm for Pd(II) in the acidic melt is shifted from the vapor phase value of 249 nm.<sup>23</sup> Also, a shoulder at 350-355 nm is seen for the acidic melt species which is not observed for the vapor phase complex. Therefore, although we believe Pd(II) exists as a square planar chloroaluminate species in the acidic melt, possibly Pd(AlCl<sub>4</sub>)<sub>2</sub><sup>(2-n)-</sup>, we cannot make a definitive structural assignment with the current spectral data.

### Conclusion

Palladium provides an interesting study of the behavior of metal chlorides in the chloroaluminate room temperature molten salts. In basic melts, Pd(II) is deposited as Pd(0) and stripped in a process involving surface and bulk oxidation. In acidic and neutral melts, the palladium electrochemistry is dominated by surface processes due to the low solubility of Pd(II) in these melts. On oxidation, the surface of a palladium electrode or of electrodeposited palladium is passivated by formation of an insoluble palladium chloride

layer between 0.5 and 2.0 monolayers thick. This behavior is similar to palladium electrochemistry in aqueous solutions where palladium forms passivating oxide/hydroxides on the surface.

### Acknowledgment

This work was supported by the Air Force Office of Scientific Research.

Manuscript submitted Sept. 3, 1993; revised manuscript received Dec. 14, 1993.

The United States Air Force Academy assisted in meeting the publication costs of this article.

### REFERENCES

- R. A. Osteryoung, in *Molten Salt Chemistry*, G. Mamtov and R. Marassi, Editors, p. 329, D. Reidel Publishing, Holland (1987).
- R. L. Vaughn, FJSRL-TR-90-0001, Frank J. Seiler Research Laboratory, USAF Academy, CO (April 1990).
- C. L. Hussey, *Pure Appl. Chem.*, **60**, 1763 (1988).
- X.-H. Xu and C. L. Hussey, *This Journal*, **139**, 1295 (1992).
- A. J. Bard and L. R. Faulkner, *Electrochemical Methods*, Chap. 12, John Wiley & Sons, Inc., New York (1980).
- I.-W. Sun and C. L. Hussey, *J. Electroanal. Chem.*, **214**, 325 (1989).
- H. C. De Long and J. S. Wilkes, in *Molten Salts*, R. J. Gale and G. Blomgren, Editors, PV 92-16, p. 465, The Electrochemical Society Proceedings Series, Pennington, NJ (1992).
- H. C. De Long and R. T. Carlin, in *Molten Salt Chemistry and Technology*, M.-L. Saboungi and H. Kojima, Editors, PV 93-9, p. 358, The Electrochemical Society Proceedings Series, Pennington, NJ (1993).
- L. D. Burke and J. K. Casey, *This Journal*, **140**, 1284 (1993).
- L. D. Burke and J. K. Casey, *ibid.*, **140**, 1292 (1993).
- M.-C. Jeong, C. H. Pyun, and I.-H. Yeo, *ibid.*, **140**, 1986 (1993).
- J. S. Wilkes, J. A. Levisky, R. A. Wilson, and C. L. Hussey, *Inorg. Chem.*, **21**, 1263 (1982).
- T. J. Melton, J. Joyce, J. T. Maloy, J. A. Boon, and J. S. Wilkes, *This Journal*, **137**, 3865 (1990).
- T. A. Zawodzinski, Jr., R. T. Carlin, and R. A. Osteryoung, *Anal. Chem.*, **59**, 2639 (1987).
- M. A. M. Noël, P. C. Trulove, and R. A. Osteryoung, *ibid.*, **63**, 2892 (1991).
- H. C. De Long, Unpublished results.
- Southampton Electrochemistry Group, *Instrumental Methods in Electrochemistry*, Chap. 9, Ellis Horwood Limited, Chichester (1985).
- A. F. Wells, *Structural Inorganic Chemistry*, 5th ed., Chap. 29, p. 1288, Oxford University Press, Oxford (1984).
- Z. Stojek and J. Osteryoung, *Anal. Chem.*, **63**, 839 (1991).
- J. W. Schultze, M. M. Lohrengel, and D. Ross, *Electrochim. Acta*, **28**, 973 (1983).
- C. K. Jorgenson, *Absorption Spectra and Chemical Bonding in Complexes*, Pergamon Press, Oxford (1962).
- A. J. McCafferty, P. N. Schatz, and P. J. Stephens, *J. Am. Chem. Soc.*, **90**, 5730 (1968).
- G. N. Papatheodorou, in *Current Topics in Materials Science*, E. Kalidis, Editor, Vol. 10, p. 249, North-Holland Publishing Amsterdam (1982).

Accession For	
NTIS GRA&I	<input checked="" type="checkbox"/>
DTIC TAB	<input type="checkbox"/>
Unannounced	<input type="checkbox"/>
Justification	
By	
Distribution/	
Availability Codes	
Dist	Avail and/or Special
A-1	201

